XVIII International Conference on Water Resources
CMWR 2010
J. Carrera (Ed)

A CONTROL VOLUME MIXED FINITE ELEMENT FORMULATION FOR TRIANGULAR ELEMENTS

Richard L. Naff

U.S. Geological Survey, Denver, CO USA
e-mail: rlnaff@usgs.gov

Key words: Mixed methods, mixed finite element, control volume, Darcy flow

Summary. A control volume mixed finite element scheme for a triangular discretization of a 2-D domain is presented; several control-volume scenarios for use with the scheme are explored.

1 INTRODUCTION

In this paper, a mixed variational approach in conjunction with the Control Volume Mixed Finite Element (CVMFE) method is used to derive flux and pressure equations over a domain descritized with triangular elements. In the CVMFE method, it is customary to construct a control volume $\bar{Q}$ which straddles the common edge or face between two adjoining elements T_i and T_j. The control volume $\bar{Q}$ is constructed such that $\bar{Q} = Q_i \cup Q_j$ where $Q_i \subset T_i$ and $Q_j \subset T_j$ and Q_i and Q_j join at the common face (see Figure 1a). The objective is to construct, by integrating over an appropriate control volume, a discrete form of the Darcy relation which defines the relation between the discrete pressures and fluxes. Comparisons are made with the Standard Mixed Finite Element (SMFE) method for triangular elements[1] using results from modelling a rough-coefficient scenario. The CVMFE derivation presented herein uses reference space in preference to real space; the equivalency of the two spaces is frequently noted in the mixed finite element literature[2,3].

2 BASIC EQUATIONS

Mass conservation for 2-D steady flow in a permeable medium can be written

$$\nabla \cdot \mathbf{q} \;=\; W(x,y), \qquad (x,y) \in \Omega \tag{1}$$

where $\mathbf{q}$ is the specific discharge vector and W is a source term. Boundary conditions on the surface $\partial\Omega$ are fluxes over $\partial\Omega_f$ and/or specified pressures over $\partial\Omega_p$; otherwise $\partial\Omega$ is considered an impermeable boundary. The Darcy relation is assumed to link the pressure p to the specific discharge $\mathbf{q}$:

$$\mathbf{q} \;=\; -\mathbf{K}\,\nabla p \tag{2}$$

where $\mathbf{K}(x,y) = \boldsymbol{\kappa}(x,y)/\gamma$, $\boldsymbol{\kappa}(x,y)$ is the hydraulic conductivity tensor, and γ is the specifc weight of water (taken constant); $\mathbf{K}$ has units $L^4T^{-1}F^{-1}$. In the CVMFE method the inverse of $\mathbf{K}(x,y)$ is used, so the operational equation becomes

$$\nabla p \;=\; -\,\mathbf{K}^{-1}\,\mathbf{q}. \tag{3}$$

The domain Ω is assumed discretized with a mesh of trangular elements referenced by Cartesian coordinates $\mathbf{r} = (x,y)$. Each element T_i is the image under a bilinear mapping of an equilateral triangle $\hat{T}_i$ in which the sides all have unit length (Figure 1b). The reference triangle $\hat{T}_i$ is positioned with regard to local coordinates $\boldsymbol{\rho} = (\eta,\xi)$ and is defined by vertices $\boldsymbol{\rho}_1 = (0,\sqrt{3}/2)$, $\boldsymbol{\rho}_2 = (1/2,0)$ and $\boldsymbol{\rho}_3 = (-1/2,0)$. The mesh element T_i is defined by the location of its vertices at $\mathbf{r}_1 = (x_1,y_1)$, $\mathbf{r}_2 = (x_2,y_2)$ and $\mathbf{r}_3 = (x_3,y_3)$; these vertices map into the correspondingly numbered reference vertices $\boldsymbol{\rho}_1$, $\boldsymbol{\rho}_2$ and $\boldsymbol{\rho}_3$. A

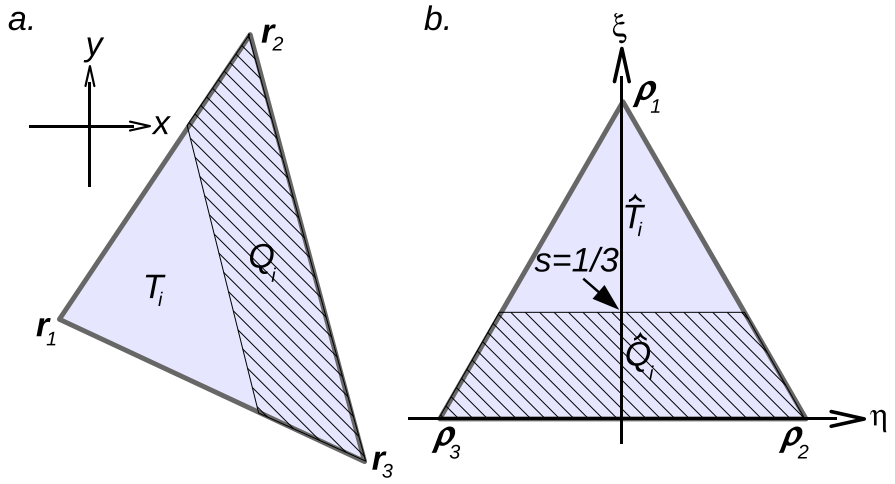

Figure 1: **a.** triangular element T_i from discretization with vertex locations $\mathbf{r}_1$, $\mathbf{r}_2$ and $\mathbf{r}_3$. Hatched area denotes control volume Q_i. **b.** equilateral reference triangle $\hat{T}_i$ with edges of unit length. Hatched area denotes reference control volume $\hat{Q}_i$.

mapping that associates with any reference location $\boldsymbol{\rho} = (\eta,\xi)$ in $\hat{T}$ with a point $\mathbf{r} = (x,y)$ in T is:

$$\mathbf{r} \;=\; \mathbf{v}_i + \boldsymbol{\Psi}_i\eta + \boldsymbol{\Sigma}_i\xi \tag{4}$$

where $\mathbf{v}_i = (\mathbf{r}_2 + \mathbf{r}_3)/2$, $\boldsymbol{\Psi}_i = \mathbf{E}_{23}$, $\boldsymbol{\Sigma}_i = \sqrt{3}(\mathbf{E}_{12} + \mathbf{E}_{13})/3$, and where $\mathbf{E}_{ij} = \mathbf{r}_i - \mathbf{r}_j$ are edge vectors.

3 SHAPE FUNCTION AND SPECIFIC DISCHARGE

The vector shape functions are used to approximate the specific discharge $\mathbf{q}$ within any given triangular element T_i using the bulk fluxes f_k crossing faces F_k (Figure 2a).

Allowing $\hat{\mathbf{q}}$ to be an approximation of $\mathbf{q}$ over element T_i, then $\hat{\mathbf{q}}$ takes the form

$$\hat{\mathbf{q}} \;=\; f_1\boldsymbol{\nu}_{i1} \;+\; f_2\boldsymbol{\nu}_{i2} \;+\; f_3\boldsymbol{\nu}_{i3} \tag{5}$$

where $\boldsymbol{\nu}_{ik}$ represents the vector shape function for face F_k. With regard to reference space

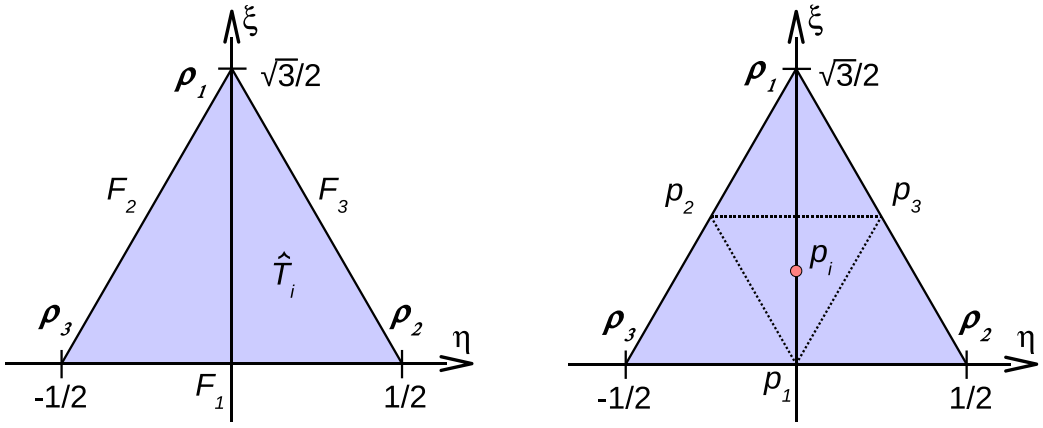

a. Face designation. **b.** Pressure support.

Figure 2: **a.** Reference triangle $\hat{T}_i$ showing arrangement of faces F_k. **b.** Reference triangle $\hat{T}_i$ showing linear pressure support (dashed triangle).

$\hat{T}_i$, the vector shape functions can be written as follows:

$$\boldsymbol{\nu}_{i1} \;=\; \frac{2\sqrt{3}}{3}\frac{\varsigma_{i1}}{J_i}\left[\boldsymbol{\Sigma}_i\left(\frac{\sqrt{3}}{2}-\xi\right)-\boldsymbol{\Psi}_i\eta\right] \tag{6a}$$

$$\boldsymbol{\nu}_{i2} \;=\; \frac{2\sqrt{3}}{3}\frac{\varsigma_{i2}}{J_i}\left[\boldsymbol{\Psi}_i\left(\frac{1}{2}-\eta\right)-\boldsymbol{\Sigma}_i\xi\right] \tag{6b}$$

$$\boldsymbol{\nu}_{i3} \;=\; -\frac{2\sqrt{3}}{3}\frac{\varsigma_{i3}}{J_i}\left[\boldsymbol{\Psi}_i\left(\frac{1}{2}+\eta\right)+\boldsymbol{\Sigma}_i\xi\right] \tag{6c}$$

where $J_i = 4\sqrt{3}A_i/3$ is the Jacobian for mapping (4), A_i is the area of triangular element T_i and ς_{i1} is a sign element which is positive for an inward flux scenario and negative for an outward flux scenario.

A discrete flux divergence relation is developed for an arbitrary triangle T_i by applying Gauss's divergence theorm to (1). Assuming that $\mathbf{q}$ in (1) can be replaced with $\hat{\mathbf{q}}$ of (5), then integrating $\nabla\cdot\mathbf{q}$ over T_i gives the result

$$\int_{T_i}\nabla\cdot\mathbf{q}\,dv \;=\; \int_{\partial T_i}\mathbf{q}\cdot\mathbf{n}\,ds \;\approx\; \int_{\partial\hat{T}_i}\hat{\mathbf{q}}\cdot\mathbf{n}\,d\hat{s} \;=\; -\left[\varsigma_{i1}f_1 \;+\; \varsigma_{i2}f_2 \;+\; \varsigma_{i3}f_3\right] \tag{7}$$

where $\mathbf{n}$ is the outward unit normal as defined on faces F_k of T_i. Thus, a form for the discrete flux divergence is

$$\varsigma_{i1} f_1 \; + \; \varsigma_{i2} f_2 \; + \; \varsigma_{i3} f_3 \; = \; - \int_{T_i} W(x,y)\, dv. \tag{8}$$

4 TEST FUNCTION AND PRESSURE GRADIENT

In this section, the application of the vector test function to the pressure gradient (3) within an arbitrarily triangular element i is examined. In contrast to the application of CVMFE for quadrilateral elements[2], it is not obvious that the control-volume boundary should pass through the element centroid; rather, the possibility exists that this boundary could be located at any point along the ξ axis such that $\xi = s\sqrt{3}/2$, where $0 < s \leq 1$ (Figure 1b). Control-volume boundaries corresponding to the centroid location ($s = 1/3$), the half distance between the base and vertex of the triangular element ($s = 1/2$), and the full element ($s = 1$) are investigated. In addition to these somewhat logical locations, a location at $s = 1/4$ will be included to test the effect of using a smaller control volume.

The vector test function $\boldsymbol{\omega}_i$ for the CVMFE method is taken directly from the covariant vector $\boldsymbol{\Sigma}_i = \partial \mathbf{r}/\partial \xi$ in (4), and is defined as[3,4]

$$\boldsymbol{\omega}_i \; = \; \frac{\upsilon(s) \boldsymbol{\Sigma}_i}{J_i}, \qquad \frac{1}{\upsilon(s)} \; = \; 2\sqrt{3} \int_0^{s\sqrt{3}/2} \int_{\frac{\sqrt{3}}{3}\xi - \frac{1}{2}}^{-\frac{\sqrt{3}}{3}\xi + \frac{1}{2}} d\eta \, d\xi \tag{9}$$

where J_i is the the Jacobian defined in (6), and $\upsilon(s)$ is the control volume coverage factor. A linear pressure support for p within T_i is assumed (Figure 2b):

$$p \; = \; (1 - \frac{4\sqrt{3}}{3}\xi) p_1 \; + \; \frac{2\sqrt{3}}{3}(\xi - \sqrt{3}\eta) p_2 \; + \; \frac{2\sqrt{3}}{3}(\xi + \sqrt{3}\eta) p_3 \tag{10}$$

where p_1, p_2, p_3 are the edge pressures for T_i. The derivative of p with respect to the ξ coordinate is simply

$$\frac{\partial p}{\partial \xi} \; = \; 2\sqrt{3}(p_i - p_{i1}), \qquad p_i \; = \; p|_{\eta = 0, \xi = \sqrt{3}/6} \; = \; (p_1 + p_2 + p_3)/3 \tag{11}$$

where $p_{i1} = p_1$ is the edge pressure on F_1 for $\hat{T}_i$, as illustrated in Figure 2b.

With regard to the left-hand side of (3), the dot product of the pressure gradient ∇p and the test function (9) is integrated over the control volume for triangular element T_i. Noting that covariant vectors Σ_i and Ψ_i in T_i become unit vectors in $\hat{T}_i$ and therefore that $\nabla p \cdot \boldsymbol{\Sigma}_i = \partial p / \partial \xi$, then a discrete pressure gradient is obtained:

$$\begin{aligned} \int_{Q_i} \nabla p \cdot \boldsymbol{\omega}_i \, dv \; &= \; \int_0^{s\sqrt{3}/2} \int_{\frac{\sqrt{3}}{3}\xi - \frac{1}{2}}^{-\frac{\sqrt{3}}{3}\xi + \frac{1}{2}} \nabla p \cdot \boldsymbol{\omega}_i J_i \, d\eta \, d\xi \\ &= \; \upsilon(s) \int_0^{s\sqrt{3}/2} \int_{\frac{\sqrt{3}}{3}\xi - \frac{1}{2}}^{-\frac{\sqrt{3}}{3}\xi + \frac{1}{2}} \frac{\partial p}{\partial \xi} \, d\eta \, d\xi \; = \; p_i - p_{i1}. \end{aligned} \tag{12}$$

5 DISCRETE DARCY RELATION

The discrete Darcy relation is established by first integrating (3) over $\hat{Q}_i$ with respect to the test function (9), and then joining that result to an equivalent integration over $\hat{Q}_j$ associated with the adjoining T_j. Replacing $\mathbf{q}$ with $\hat{\mathbf{q}}$ on the right-hand side of (3), then

$$-\int_{Q_i} \boldsymbol{\omega}_i \cdot \mathbf{K}_i^{-1}\mathbf{q}\, dv \;\approx\; -\sum_{k=1}^{3} f_k \int_{\hat{Q}_i(s)} \boldsymbol{\omega}_i \cdot \mathbf{K}_i^{-1}\boldsymbol{\nu}_{ik}\, d\hat{v} \;=\; -\sum_{k=1}^{3} \varsigma_{ik} a_{ik}\, f_k. \tag{13}$$

For the purposes of this study, it is assumed that $\mathbf{K}_i^{-1}$ is a tensor constant with respect to T_i. After evaluation, the coefficients a_{ik} in (13) become:

$$a_{i1}(s) \;=\; \alpha(s)\left[\boldsymbol{\Sigma}_i \cdot \mathbf{K}_i^{-1}\boldsymbol{\Sigma}_i\right]/A_i \tag{14a}$$

$$a_{i2}(s) \;=\; \beta(s)\left[\phi(s)\,\boldsymbol{\Sigma}_i \cdot \mathbf{K}_i^{-1}\boldsymbol{\Psi}_i - \boldsymbol{\Sigma}_i \cdot \mathbf{K}_i^{-1}\boldsymbol{\Sigma}_i\right]/A_i \tag{14b}$$

$$a_{i3}(s) \;=\; -\beta(s)\left[\boldsymbol{\Sigma}_i \cdot \mathbf{K}_i^{-1}\boldsymbol{\Sigma}_i + \phi(s)\,\boldsymbol{\Sigma}_i \cdot \mathbf{K}_i^{-1}\boldsymbol{\Psi}_i\right]/A_i \tag{14c}$$

where $\alpha(s)$, $\beta(s)$ and $\phi(s)$ are parameters dependent on the coverage s of the element, and A_i is the element area as noted in (6). Equating (12) and (13), the local discrete Darcy relation for the triangular element T_i can be written

$$p_i - p_{i1} \;=\; -\sum_{k=1}^{3} \varsigma_{ik} a_{ik}\, f_{ik} \tag{15}$$

where p_{i1} is the edge pressure given in (11), f_{ik} is the bulk flux across F_k in T_i. For a triangular element T_j adjoining element T_i at face F_1 (see Figures 1 and 2a), the local discrete Darcy relation can similarly be written

$$p_j - p_{j1} \;=\; -\sum_{k=1}^{3} \varsigma_{jk} a_{jk}\, f_{jk} \tag{16}$$

where coefficents a_{jk} are idential in form to a_{ik} of (14) with the j index replacing the i. That flux continuity be maintained between T_i and T_j requires $\varsigma_{i1} = -\varsigma_{j1}$ and $p_{i1} = p_{j1}$; replacing ς_{j1} in (16) with $-\varsigma_{i1}$ and adding (16) and (15) eliminates the edge pressures from the discrete Darcy relation:

$$p_i - p_j \;=\; -[\varsigma_{i1}(a_{i1} + a_{j1})f_{i1} \;+\; \varsigma_{i2}a_{i2}\, f_{i2} \;+\; \varsigma_{i3}a_{i3}\, f_{i3} \;-\; \varsigma_{j2}a_{j2}\, f_{j2} \;-\; \varsigma_{j3}a_{j3}\, f_{j3}]. \tag{17}$$

The coefficients α, β and ϕ, found in (14) have the following values: for $s = 1/4$: $\alpha = 37/336$, $\beta = 5/336$, and $\phi = 14\sqrt{3}/5$; for $s = 1/3$: $\alpha = 19/180$, $\beta = 7/360$, and $\phi = 15\sqrt{3}/7$; for $s = 1/2$: $\alpha = 7/72$, $\beta = 1/36$, and $\phi = 3\sqrt{3}/2$; and for $s = 1$: $\alpha = 1/12$, $\beta = 1/24$, and $\phi = \sqrt{3}$.

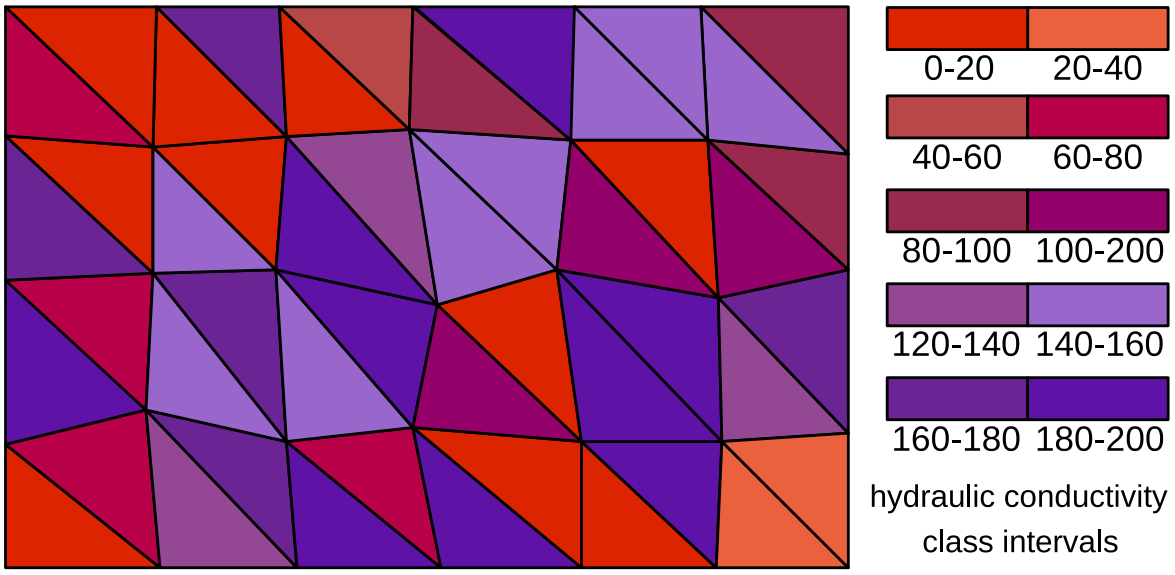

Figure 3: Mesh for irregular grid, consisting of 48 triangular elements in which vertex locations have been randomly perturbed. Values for $\mathbf{K}(x, y)$, in units consistant with (2), are given at right.

6 RESULTS AND DISCUSSION

Discrete equations (8) and (17) can be assembled into the following matrix equation:

$$\begin{bmatrix} M & N^T \\ N & 0 \end{bmatrix} \begin{bmatrix} f \\ p \end{bmatrix} = \begin{bmatrix} r_f \\ r_p \end{bmatrix} \tag{18}$$

where $M = \{a_{ik}\}$, $N = \{\varsigma_{ik}\}$, $r_f = \{p_l^b\} - \{a_{il} f_l^b\}$, and $r_p = -\{\varsigma_{il} f_l^b\} - \{\int_{T_i} W(x, y)\, d\mathbf{v}\}$, and where f_l^b and p_l^b represent specified flux and pressure conditions, respectively. These equations are solved by the Schur complement method[1]; while this method isn't particularly efficient, it is relatively easily implemented.

If the hydraulic conductivity field is homogeneous, experience thus far indicates that using either the SMFE method or one of the CVMFE methods to construct the coefficients in M has little effect on the resulting solution of a given problem. Therefore, a simulation with rough coefficients was devised to compare SMFE and CVMFE methods and also to compare the CVMFE method at various levels of coverage, s. Simulations were run using the irregular mesh and the rather large hydraulic conductivity contrast depicted in Figure 3. The mesh was refined by subdividing each triangular element into four triangles by connecting the midpoints of each element edge. Three additional refinements were performed for a maximum of 3072 elements. A uniform inward flux was imposed on the left-hand side of the domain, and an equivalent outward flux was imposed on the right-hand side; the flux rate was 0.5 L/T units consistant with $\boldsymbol{\kappa}$ of (2). Simulations were performed using coefficients for SMFE and for CVMFE with coverages of

MFE type	grid refinement			
	1×	4×	16×	64×
CVMFE: $s = \frac{1}{2}, \frac{1}{3}, \frac{1}{4}$ & SMFE	4.282×10^{-02}	2.467×10^{-02}	1.588×10^{-02}	7.588×10^{-03}
CVMFE: $s = 1$	4.282×10^{-02}	2.467×10^{-02}	1.589×10^{-02}	3.047

Table 1: Approximate Flux $\mathcal{L}^2$ norm $\|\mathbf{f}\|_\mathbf{2}$ for rough-coefficient simulations as function of simulation type and grid refinement. Refinement 1×: 48 elements. Subsequent refinements contain four times as many elements as the previous refinement.

$s = 1/4,\ 1/3,\ 1/2,$ and 1. Flux accuracy was measured using the $\mathcal{L}^2$ norm, defined herein as

$$\|\mathbf{f}\|_2 \ = \ \left\{ \sum_i \bar{Q}_i \left[(\tilde{f}_i - f_i)/L_i \right]^2 \Big/ \sum_i \bar{Q}_i \right\}^{1/2} ,$$

where, for all faces $F_i \in \Omega$, $\tilde{f}_i$ and f_i are the estimated and "true" fluxes, respectively, L_i is the length of face F_i, and $\bar{Q}_i$ is a control volume straddling F_i (the choice of s is immaterial in this case). Estimates of the "true" fluxes f_i were obtained from a SMFE solution using a fourth-level grid refinement consisting of 12,288 elements. The SMFE method was chosen for this purpose after a comparison of flux results from the third-level grid refinement level (3072 elements) revealed that the CVMFE method with $s = 1$ produced fluxes dissimilar to fluxes obtained from the SMFE method and CVMFE method with $s = 1/4,\ 1/3,\ 1/2$, while the SMFE method and CVMFE method with $s = 1/4,\ 1/3,\ 1/2$ all produced fluxes that were quite similar. Table 1 is a compilation of $\|\mathbf{f}\|_2$ results for the various solution methods and grid refinements. Notable here are the CVMFE method results with $s = 1$; the abrupt increase in $\|\mathbf{f}\|_2$ with increased grid refinement is rather dramatic, indicating that CVMFE with $s = 1$ is an inferior approximation. Otherwise, the solution quality improves at best linearly with each mesh refinement.

Upon consideration of the $\mathcal{L}^2$ norm results, a decision was made to investigate the condition number κ of the matrix M in (18) for the various methods and grid refinements. The condition number used herein is defined[5] as $\kappa = \|M\|_\infty \|M^{-1}\|_\infty$, where, for any matrix A, $\|A\|_\infty = \max_{1 \le i \le n} \sum_{j=1}^{n} |a_{ij}|$. Condition number results are contained in Table 2; the second column in this table, labelled κ_{smfe}, contains the actual condition numbers for the SMFE method, and columns three through six contain the condition numbers for the CVMFE method, for various coverages s, expressed as the ratio $\kappa_{\text{cvmfe}}/\kappa_{\text{smfe}}$. Most notable here are the rather large condition numbers associated with the CVMFE method when $s = 1$; the degradation with increased grid refinement is most pronounced, but even for 1× refinement, κ_{cvmfe} is nearly three times larger than κ_{smfe}. This result suggests that using the entire element as the basis for the control volume in the CVMFE method is not appropriate. The condition numbers for the other coverages were not as large as

grid refine-ment	κ_{smfe}	$\kappa_{\text{cvmfe}}/\kappa_{\text{smfe}}$ as function of coverage s			
		1/4	1/3	1/2	1
1×	261.6	1.11	1.14	1.27	2.80
4×	1156	1.08	1.10	1.25	3.98
16×	2463	1.09	1.11	1.27	6.92
64×	5073	1.08	1.11	1.27	12.9

Table 2: Condition number for matrix M. κ_{smfe}: condition number for SMFE matrix. κ_{cvmfe}: condition number for CVMFE matrix. Refinement 1×: 48 elements. Subsequent refinements contain four times as many elements as the previous refinement.

those for $s = 1$ and maintain a near-constant ratio with κ_{smfe} even as grid refinement increases matrix size. For $s = 1/4$ and $1/3$, the condition numbers are about 10% larger than κ_{smfe}. While the condition numbers for the CVMFE method do decrease with decreasing s, the slight amount of change between $s = 1/4$ and $s = 1/3$ suggests that little would be gained by further decreasing the coverage s.

7 CONCLUSIONS

For the rough-coefficient test herein, the CVMFE method performed best if coverage s is limited to smaller values ($s = 1/4$, $s = 1/3$). The CVMFE method does have a slight disadvantage to the SMFE method with regard to the condition number of matrix M.

References

[1] L. J. Durlofsky. A triangle based mixed finite element - finite volume technique for modeling two phase flow through porous media. *J. Comput. Phys.*, 105:252–266, (1993).

[2] Z. Cai, J. E. Jones, S. F. McCormick, and T. F. Russell. Control volume mixed finite element methods. *Computational Geosciences*, 1:289–315, (1997).

[3] R.A. Klausen and T.F. Russell. Relationships among some locally conservative discretization methods which handle discontinuous coefficients. *Computational Geosciences*, 8(4):341–347, (2005).

[4] R. L. Naff, T. F. Russell, and J. D. Wilson. Test functions for three-dimensional control-volume mixed finite-element methods on irregular grids. In *Proceedings XIII International Conference on Computational Methods in Water Resources*, pages 677–684. A. A. Balkema, (2000).

[5] G. H. Golub and C. F. Van Loan. *Matrix Computations*. Johns Hopkins University Press, Baltimore, third edition, (1996).